Pi7, an Orphan Peptide from the Scorpion *Pandinus imperator*: A ^{1}H-NMR Analysis Using a Nano-NMR Probe[†,‡]

M. Delepierre,*[,§] A. Prochnicka-Chalufour,[§] J. Boisbouvier,[||] and L. D. Possani[⊥]

Laboratoire de RMN Institut Pasteur, CNRS URA 1129, 28 rue du Dr. Roux, 75724, PARIS Cedex 15, France, Institut de Biologie Structurale Jean-Pierre EBEL (CEA-CNRS), 41 rue Jules Horowitz38027 GRENOBLE Cedex 1, France, and Department of Molecular Recognition and Structural Biology, Institute of Biotechnology, National Autononous University of Mexico, Av. Universidad, 2001 Cuernavaca, Mexico 62271

Received July 21, 1999; Revised Manuscript Received October 8, 1999

ABSTRACT: The three-dimensional solution structure of a novel peptide, Pi7, purified from the venom of the scorpion *Pandinus imperator*, and for which no specific receptor has been found yet, was determined by two-dimensional homonuclear proton NMR methods from a nanomole amount of compound using a nano-nmr probe. *Pandinus imperator* peptide 7 does not block voltage-dependent K^+-channels and does not displace labeled noxiustoxin from rat brain synaptosomal membranes. The toxin has 38 amino acid residues and, similarly to Pi1, is stabilized by four disulfide bridges (Cys6-Cys27, Cys12-Cys32, Cys16-Cys34, and Cys22-Cys37). In addition, the lysine at position 26 crucial for potassium-channel blocking is replaced in Pi7 by an arginine. Tyrosine 34, equivalent to Tyr36 of ChTX is present, but the N-terminal positions 1 and 2 are occupied by two acidic residues Asp and Glu, respectively. The dihedral angles and distance restraints obtained from measured NMR parameters were used in structural calculations in order to determine the conformation of the peptide. The disulfide-bridge topology was established using distance restraints allowing ambiguous partners between S atoms combined with NMR-derived structural information. The structure is organized around a short α-helix spanning residues Thr9 to Thr20/Gly21 and a β-sheet. These two elements of secondary structure are stabilized by two disulfide bridges, Cys12-Cys32 and Cys16-Cys34. The antiparallel β-sheet is composed of two strands extending from Asn22 to Cys34 with a tight turn at Ile28-Asn29 in contact with the N-terminal fragment Ile4 to Cys6.

Scorpion venoms are rich sources of different classes of peptides that affect the function of ion channels (*1*). These peptides disrupt the normal function of excitable tissues found in muscles and nerves of many animals, including man, by causing respiratory and circulatory damages that can eventually lead to death. Apart from the important public health problem caused by scorpion stings in certain areas of the world (*2*), these peptides represent useful tools for biological research; mainly that concerning cellular excitability and ion channels (*3*).

Toxins affecting potassium channels have only minor contribution to human intoxication; however, they have been successfully used to characterize K^+-channels (*4*−*7*) among which the *Streptomyces lividans* K^+-channel had its three-dimensional structure solved (*8*).

The potassium channel specific toxins can act on: (i) the voltage-dependent potassium channels (Kv types, Shaker), (ii) the large conductance, calcium-activated potassium channels (maxi-K or BK-type), (iii) the small conductance calcium-dependent potassium channels or apamin sensitive (insectotoxins), and (iv) Herg-channels from heart and other tissues (*9*). The first isolated toxin specific for K^+-channels was noxiustoxin (NTX) (*10*) and its solution structure was solved only recently (*11*). After NTX, a large number of homologous peptides were isolated from scorpion venoms and were shown to bind or modify the function of a variety of K^+-channels, with different specificities (Figure 1). Thus far, all known and characterized toxins, specific for mammalian K^+-channels share amino acid sequence similarities and fall into nine groups (*12*−*14*), except ergtoxin, which seems to be quite different (*9*). Among these groups, subfamily 6, for which five different members were identified, is characterized by the presence of an additional disulfide bridge and display very different toxicity and activity (*15*). Although the molecular basis of toxin specificity has been widely studied, much knowledge is still needed to fully understand their structural and functional characteristics. Small differences, such as single amino acid substitutions within or near the critical binding region of the toxin, are important for receptor recognition and modification of

[†] The work in Mexico was supported in part by grants of Howard Hughes Medical Institute (75191−527104) and the National University of Mexico (DGAPA-IN217997) to LDP. The work in Paris was supported by funds from the Pasteur Institute and the Centre National de la Recherche Scientifique (URA 1129). The work in Grenoble was supported by the Commissariat à l'Energie Atomique, the Centre National de la Recherche Scientifique, and Molecular Simulations Inc. (San Diego, CA.).

[‡] Coordinate of Pi7 has been deposited in the PDB Data Bank code: 1QKY. Chemical shifts have been deposited in the BioMagResBank under accession number: 4427.

[§] Laboratoire de RMN Institut Pasteur.

[||] Institut de Biologie Structurale Jean-Pierre.

[⊥] National Autononous University of Mexico.

* Correspondence to: M. Delepierre, Institut Pasteur, Laboratoire de Résonance Magnétique Nucléaire, 28 rue du Dr. Roux, 75015 Paris, France. E-mail: murield@pasteur.fr.

10.1021/bi991685m CCC: $18.00
Published on Web 12/03/1999

```
ChTX        pEFTNVSCTTSKE-CWSVCQRLHNTSRG-KCMNKKCRCYS
IbTX        pEFTDVDCSVSKE-CWSVCKDLFGVDRG-KCMGKKCRCYQ
Lq2         pEFTQESCTASNQ-CWSICKRLHNTNRG-KCMNKKCRCYS
LbTX        -VFIDVSCSVSKE-CWAPCKAAVGTDRG-KCMGKKCKCY?

ClTX1       -ITINVKCT-SPQQCLRPCKDRFGQHAGGKCINGKCKCYP
MgTX        -TIINVKCT-SPKQCLPPCKAQFGQSAGAKCMNGKCKCYPH
NTX         -TIINVKCT-SPKQCSKPCKELYGSSAGAKCMNGKCKCYNN-NH2
NTX2        -TIINEKCF-ATSQCWTPCKKAIGSLQS-KCMNGKCKCYNG

KlTX1       GVEINVKCSGSP-QCLKPCKDAGMRF-G-KCMNRKCHCTP
KlTX2       -VRIPVSCKHSG-QCLKPCKDAGMRF-G-KCMNGKCDCTP
AgTX1       GVPINVKCTGSP-QCLKPCKDAGMRF-G-KCINGKCHCTPK
AgTX2       GVPINVSCTGSP-QCLKPCKDAGMRF-G-KCMNRKCHCTPK
AgTX3       GVPINVPCTGSP-QCLKPCKDAGMRF-G-KCINGKCHCTPK

TyKα        -VFINAKCRGSPE-CLPKCKEAIGKAAG-KCMNGKCKCYP--?
TsK         -VVIGQRCYRSPD-CYSACKKLVGKATG-KCTNGRCDC----OH

ScTX        -----AFC-NLRM-CQLSCRSLG--LLG-KCIGDKCECVKH-NH2
PO5         -----TVC-NLRR-CQLSCRSLG--LLG-KCIGVKCECVKH-OH
BmPO5       -----AVC-NLKR-CQLSCRSLG--LLG-KCIGDKCECVKH-NH2

Pi1           LVKCRGTS-DCGRPCQQQTGCPNS-KCINRMCKCYGC-NH2
Pi4         IEAIRCGGSR-DCYRPCQKRTGCPNA-KCINKTCKCYGCS
Pi7         DEAIRCTGTK-DCYIPCRYITGCFNS-RCINKSCKCYGCT
MTX           -VSCTGSK-DCYAPCRKQTGCPNA-KCINKSCKCYGC-NH2
HsTX1         -ASCRTPK-DCADPCRKETGCPYG-KCMNRKCKCNRC-NH2

Pi2           TISCTNPK-QCYPHCKKETGYPNA-KCMNRKCVCFPI-?
Pi3           TISCTNEK-QCYPHCKKETGYPNA-KCMNRKCKCFGR-?

PO1         -----VSC----EDCPEHCSTQK--AQA-KCDNDKCVCEPI-OH
BmPO1       -----ATC----EDCPEHCATQN--ARA-KCDNDKCVCEPK-OH
BmPO2       -----VGC----EECPMHCKGKN--AKP-TCDDGVCNCNV--OH

CoTX1       -----AVC--VYRTCDKDCKRRG-YRSG-KCINNACKCYPY-OH
CoTX2       -----VAC--VYRTCDKDCTSRK-YRSG-KCINNACKCYPY-OH
```

FIGURE 1: Comparison of amino acid sequences and disulfide pairing of Pi7 (PI) with other related potassium channel toxins. The sequences are taken from review by Selisko et al. (*14*), Pi4 and Pi7 (*17*). Gaps were introduced to enhance identity. The important lysine for channel binding is indicated in light blue, the conserved cysteines are in red, while the additional cysteines are in green.

channel function. Thus, comparative studies of structuraly similar toxins that display different affinities or effectiveness toward their target receptors (ion-channels) would help to highlight the crucial residues involved in their molecular interactions.

Here, we describe the solution structure of a new peptide, Pi7 isolated from the venom of the scorpion *Pandinus imperator*, a Scorpionidae from the Chactoidae subgroup (*16*), not dangerous to humans. The peptide has 38 amino acid residues (*17*) and it is cross-linked by four disulfide bridges. Pairings of cysteines at positions 6−27, 12−32, and 16−34 correspond to the usual pattern found in short-chain scorpion toxins. The disulfide bridge at position Cys22-Cys37 is the novel structural characteristic of this peptide. Pi7 is not active, even at 0.3 μM concentration on shaker B potassium channels, a voltage-dependent channel, and does not displace NTX binding from synaptosomal membranes at 0.1 μM concentration (*17*). This is quite surprising, since most K^+-channel specific toxins have affinities on the range of low nanomolar or even picomolar level, like its homologous Pi2, purified from the same scorpion venom, which affect K^+-channel in lymphocytes at the level of 50 pM (*18*).

In this manuscript, we report the Pi7 ^{1}H NMR[1] assignments, the secondary structure determination, and the

calculation of the global 3D structure. The structure obtained is compared with the structure of active peptides affecting the potassium channels and in particular with those of the same subfamily. Special attention was given to the disulfide pairing of the cysteines using a recently proposed protocol that takes into consideration the floating distance constraints between cysteines sulfur atoms, based only on NMR data (*19, 20*).

MATERIAL AND METHODS

Sample Preparation. The venom was collected and prepared in the laboratory by electrical stimulation of anesthesized animals (*21*). The *Pandinus imperator* peptide 7 was purified according to the method already described and using analytical grade chemicals only (*17*). Lyophilized Pi7, (300 μg), was dissolved in 40 μL of H_2O/D_2O, 9:1 (v/v) (Eurisotop). The sample concentration was between 0.8 and 1 mM in H_2O, and the pH of the solution was estimated to be 3−3.5. Accurate measurement of pH was not possible due to the very limited sample size. The entire NMR measurements were conducted using an unique sample of Pi7, isolated from venom extracted of approximately one hundred scorpions.

NMR Spectroscopy. ^1H NMR Experiments. ^{1}H NMR experiments, using a nano-nmr probe (Varian), were run at 500 MHz on a Varian Unity spectrometer with an on-line Sun Sparc 2 workstation. The nano-nmr probe produces high-resolution spectra from liquid samples of 40 μL spun rapidly at magic angle (*22*−*24*). The 90° pulse varied between 3.5 to 5 μs for the experiments reported here. The experimental data were processed using VNMR 5.3 program. The spectral width was 4500 or 6000 Hz for experiments in D_2O and H_2O, respectively. Spectra were referred to the water signal at 4.79 ppm at 25 °C and at 4.63 ppm at 40 °C (relative to 3-trimethylsilyl-(2,2,3,3-$^2H_4$) propionate (TMSP), the external reference). The 2D ^{1}H NMR spectra were recorded in the phase sensitive mode (*25*) with 2 or 4 K data points, depending on the spectral width, in the t_2 dimension and 512 t_1 increments. Thirty-two scans were acquired for the COSY, TOCSY, and double quantum experiments and 32 or 48 scans for the NOESY experiments. Zero-filling was applied prior to Fourier transformation and data were processed with shifted sine-bell-window functions in both dimensions, except for the COSY spectra, which were apodized with sine bell functions.

Identification of spin systems was obtained through analysis and comparison of two-dimensional COSY, Clean TOCSY (*26*−*28*), DQ (two-dimensional double-quantum spectroscopy; (*29*)), and NOESY (*30*) spectra recorded at 25, 30, 35, and 40 °C. The double quantum experiment was optimized for a 15 Hz coupling constant. TOCSY spectra were recorded using either the MLEV-17 pulse scheme preceded by a 2 ms trim pulse or adiabatic mixing sequences (*31*−*32*) for the spin lock and with 30 ms and 60 ms isotropic mixing periods.

NOESY experiments were recorded with mixing times of 80, 120, 180, 250, and 300 ms at 35 °C. Distance constraints were obtained from NOESY spectra recorded in H_2O with a mixing time of 250 ms and 35 °C. Additional distance constraints in particular those involving the aromatic protons and the Hα protons were obtained from a NOESY spectrum recorded in D_2O with 150 and 250 ms mixing times at 35 °C.

NH−CαH coupling constants were measured directly from the one-dimensional spectrum obtained with a digital resolution of 0.18 Hz per data point after one zero filling. CαH−Cβ H coupling constants were either measured directly on the Hα proton in a one-dimensional spectrum obtained in D_2O or evaluated from a NOESY spectrum recorded in D_2O.

Hydrogen exchange rates were evaluated by freeze-drying the Pi7 sample from H_2O and redissolving it in D_2O. One-dimensional experiments were acquired 30 min and 6 h after D_2O addition and then a TOCSY was run to identify the slowest exchanging protons. This allowed to group the NHs into three classes: the fast exchanging that disappeared after 30 min, the slow exchanging that were observed in the 2D-TOCSY, and all the remainings NHs falling into the intermediate exchange rate class.

Structure Calculations. The 3-dimensional structures of PI7 have been determined with the program DYANA (*33*) and subsequently refined using OPAL (*34*).

Input Data. (a) Experimental Input Data. The upper distance limits were derived from NOESY spectra (see NMR spectroscopy section). NOESY cross-peaks were assigned using the XEASY program (*35*) running on a Silicon Graphics Indy workstation. NOE intensities were evaluated from the height of the cross-peaks and the upper distance limits were calculated using CALIBA routine of DYANA.

The values of $^3J_{NH\alpha}$ coupling constraints were estimated from NOESY spectrum using the program INFIT (*36*) or directly measured on 1D spectrum. Dihedral angles deduced from $^3J_{NH\alpha}$ values were constrained within the range (−90°, −40°) for $^3J_{NH\alpha} < 5.5$ Hz, (−160°, −80°) for 8 Hz $< {}^3J_{NH\alpha} <$ 9 Hz, the latter range being narrowed to (−140°, −100°) for $^3J_{NH\alpha} > 9$ Hz. (*37*). The χ_1 angles deduced from $^3J_{H\beta H\alpha}$ values were constrained with a precision of ±30°.

(b) Additional Input Data. First disulfide bridges have been determined by amino acid sequencing of the fragments generated by enzymatic cleavage of the native protein. The disulfide bridges pattern has been independently determined with a two stages simulated annealing protocol, using experimental NMR restraints associated with ambiguous intersulfur restraints. The global fold of the protein was determined using a first simulated annealing (SA) protocol starting from randomized coordinates (*38*). At this step, only NMR data (without any information on cysteine sulfur atoms) were used. The best structures selected from their experimental energy were used as starting coordinate for the second SA protocol in which we added ambiguous intersulfur restraints to previous NMR-restraints (*19, 20*). The calculations and the following analysis have been performed using the MSI Discover program interfaced with InsightII (Version 6/97, MSI). Methodological details for structure calculations and disulfide bridge analysis will be published elsewhere (*39*).

[1] Abbreviations: NMR, nuclear magnetic resonance; 2D, two-dimensional; NOE, nuclear Overhauser effects; NOESY, NOE spectroscopy; COSY, correlated spectroscopy; TOCSY, total correlated spectroscopy; DQ-COSY, double quantum spectroscopy; rmsd, root-mean-square deviation; SA, simmulated annealing; ChTX, charybdotoxin, IbTX, iberiotoxin, KTX, kaliotoxin, MgTX, margatoxin, MTX, maurotoxin, NTX, noxiustoxin, Pi1, *Pandinus imperator* toxin 1; Pi7, *Pandinus imperator* toxin 7.

Then preliminary set of structures calculations was obtained using DYANA with the input data described in (a) through (b); 200 conformers were generated using the standard simulated annealing protocol with torsion angle dynamics. Twenty-five DYANA structures with lowest target function values, ranging from 0.17 to 0.32, were subjected to restrained energy minimization performed using the program OPAL with Amber94 force field (*40*). The calculations were carried out in vacuo with distance proportional dielectric constant. Hydrogen bonds appearing in more than 65% of the structures, involving slowly exchanging NH protons and compatible with low experimental values of the corresponding temperature coefficients, have been taken as the additional distance constraints for the final structure calculations.

Final Structure Calculations. Final structure calculations were performed using the entire set of input data described above. The twenty-five DYANA conformers were energy minimized in a shell of water molecules with a minimal thickness of 6 Å and with a dielectric constant of 1. A maximal number of 1500 iterations of conjugate gradient was performed per conformer using the set of nonmeaningless distance and angle constraints generated in last DYANA calculations. The pseudoenergy terms for distance and angle constraints were calibrated such that respective violations of 0.1 and 2.5° corresponded to an energy penalty of $k_BT/2$ at room temperature.

Structure Analysis. The structures refined with OPAL have been displayed and analyzed using the program MOLMOL (*41*) and their quality was evaluated using PROCHECK software (*42*).

RESULTS AND DISCUSSION

The sequence specific assignment of Pi7 were achieved according to a standard procedure (*43*). Spectra were recorded at four different temperatures, namely, 25, 30, 35, and 40 °C, to solve ambiguities due to overlapping signals. The one-dimensional spectrum obtained with presaturation of the water signal shows that good line shape, sensitivity and resolution can be achieved (Figure 2).

Spin-System Identification. First, the spin systems of all amino acid residues were identified via their through-bond connectivities observed in COSY, TOCSY, and double quantum experiments. The sharp sensitivity dependence of the TOCSY experiment in H_2O on spinning rate (*44*) led us to generate the spin-lock with adiabatic mixing sequences (*31, 32*). Although, the reason for this peculiar behavior is not clear yet a dramatic sensitivity improvement in signal-to-noise can be achieved as compared to conventional mixing schemes (Figure 3). Indeed, adiabatic mixing sequences show low sensitivity to RF inhomogeneity and miscalibration of the B_1 field strength (*31*).

All spin systems, with the exception of one amide proton, Asn24, could be identified by combining the through-bond information acquired at several temperatures. Aromatic ring protons were assigned using TOCSY and COSY correlations in the aromatic region and specifically assigned from the NOEs observed between ring protons and Hβ and Hα protons in NOESY spectra collected in D_2O (*43*).

Sequential Assignments. The sequential assignment was obtained using the through space connectivities NHi-NHi+1, Hαi-NHi+1, and Hβi-NHi+1 observed between neighboring residues in the NOESY spectra (Figure 4). The two unique spin systems Ala3, and Pro15 were used as starting points for the sequential assignment. The sequential amide or Hα

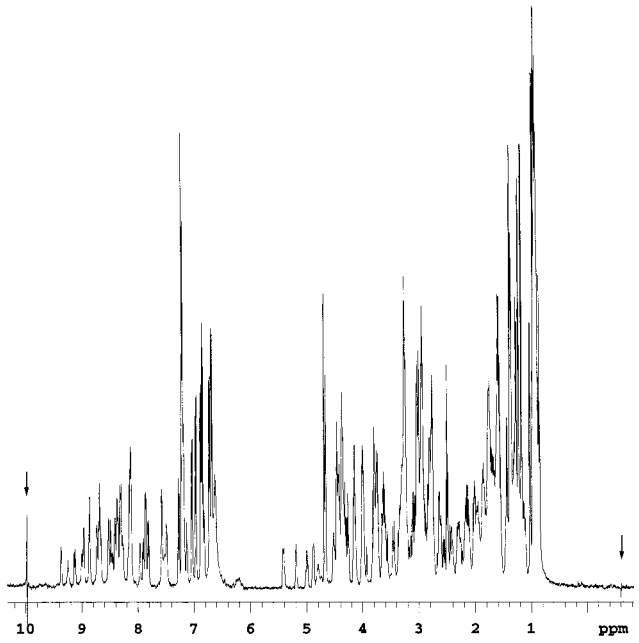

FIGURE 2: One-dimensional proton spectrum of the Pi7 toxin obtained with the nano-nmr probe. The spinning rate is 2150 Hz and the spinning sidebands are indicated with an arrow.

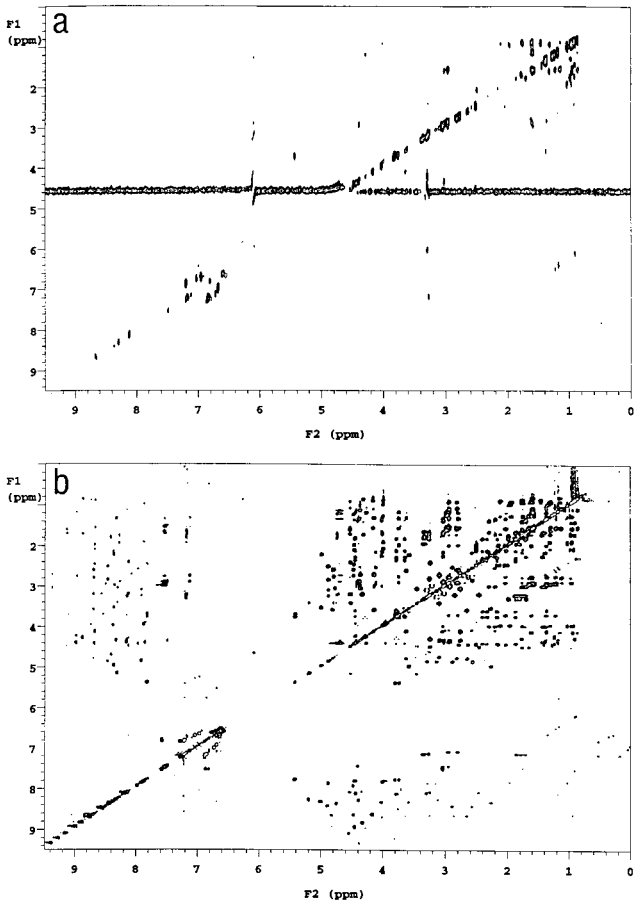

FIGURE 3: TOCSY spectra of Pi7 obtained at 35 °C in H_2O. The spinning rate is 2650 Hz. The spin lock for mixing is generated with (a) MLEV-17 pulse scheme (b) adiabatic pulse scheme.

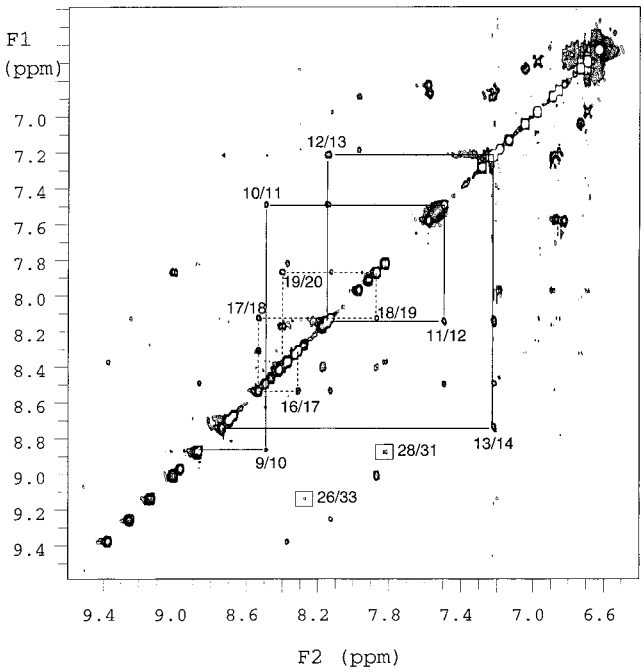

FIGURE 4: Contour plot of the amide region of the NOESY spectrum recorded with 250 ms mixing time at 35 °C. The sequential d_{NN} connectivities for residues 9−14 are illustrated by a continuous line, while dotted lines indicate d_{NN} connectivities involved in segment 16−19. The two interstrand d_{NN} interactions are boxed.

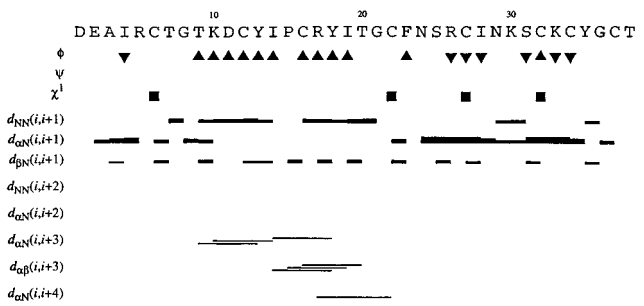

FIGURE 5: Amino acid sequence of Pi7 with summary of the NOE connectivities used in the sequential assignment procedure and secondary structure determination. Data are summed up from NOESY spectra obtained at 35 °C, pH 3.5, using a mixing time of 250 ms. For proline, sequential NOE involving $C_\delta H$ instead of NH are indicated. $^3J_{HN\alpha}$ coupling constants greater than 5.5 Hz are represented by filled triangles down, while filled triangles up correspond to coupling constants lower than 5.5 Hz.

proton NOE connectivities of Ile14 with the Hδ protons of Pro15, indicate that the Xaa-Pro amide bond is in the trans conformation. The chemical shifts of all protons of Pi7 are listed in Table S-1. It is interesting to note that the Asn24 amide proton has not been identified and that some of the Lys33 side chain protons are upfield shifted compared to their positions in random coil structures. This was also observed for the corresponding residues in Pi1 that is Asn22 and Lys31 (*23*), suggesting that the lysine protons are in close proximity to an aromatic ring. Furthermore, the two Hϵ protons of the Lys33 side chain give two distinct resonances each, implying that this side chain occupies a well-defined position in the structure.

Secondary Structure. The regular secondary structure elements are presented in Figure 5. First, the pattern of short-range NHi-NHi+1 NOEs associated with weak Hαi-NHi+1 connectivities together with the $^3J_{HN-H\alpha}$ coupling constants smaller than 5.5 Hz indicated the presence of an α helix extending from residue Thr9 to residue Thr21. Second, weak, typical medium range cross-peaks Hαi-NHi+3 (9−12 and 10−13) Hαi−Hβi+3 (14−17 and 16−19) could also be observed. The proline insertion in the middle of the helix causes some distortion in the regular pattern as shown in the slightly higher *J* values measured for some of the residues in particular for Asp11.

An antiparallel β sheet involved segments Asn24-Asn29 and Ser31-Cys34 for which strong sequential αHi-NHi+1 NOEs are observed. The two strands are connected by the Asn29-Ser31 fragment, which displays several NHi-NHi+1 connectivities characteristic of a tight turn. Indeed, two sequential NHi-NHi+1 cross-peaks detected between residues Asn29 and Lys30 and between Lys30 and Ser31 together with the weak sequential Hαi-NHi+1 interactions observed between residues Asn29 and Lys30 and between Lys30 and Ser31 suggest the presence of a type I β-turn. The very slow exchange rate of Ser31 amide proton associated with a low-temperature coefficient would suggest that an hydrogen bond is formed from this NH to the carbonyl of Ile28. A number of long-range NHi-NHj [26:33; 28:31], αHi-NHj [25:35], NHi-αHj [6:31, 6:30, and 26:33 at 25 °C] and αHi-αHj [5:31, 25:34, 27:32] connectivities suggest that the N-terminal fragment (Glu2-Cys6) is located close to the β-sheet. The lack of sufficient long-range interactions impeded exact location of strand 4−6 in the antiparallel β-sheet. Large $^3J_{HN-H\alpha}$ coupling constant values were obtained for most of the residues in the β-sheet confirming its structure. The Cys32 coupling constant is abnormally low (5 Hz), suggesting a distortion in the β-sheet structure. The smaller value obtained for the $^3J_{HN-H\alpha}$ Cys32 coupling constant was also measured for the cysteine at equivalent position in several toxins, namely, ChTX (*45*), also on ChTX lacking the 13−33 disulfide bridge (*46*) MgTX (*47*), KTX (*48*), AgTX2 (*49*), PO1 (*50*), and Pi1 (*23*), whereas for MTX (*51*) and IbTX (*52*) it was not determined.

Four Turns are Found in the Structure. The first one involves residues Thr7 and Gly8 for which a strong sequential NHi-NHi+1 effect is observed. It corresponds to the strongest interaction observed in this region. Furthermore, the weak Hαi-NHi+1 dipolar interactions between residues Cys6 and Thr7 and between residues Thr7 and Gly8 associated with the large NH−Hα proton coupling constants for residues Cys6 and Thr7 are in favor of a type II′ β-turn. This is reinforced by the low-temperature coefficient obtained for the Cys6 NH together with its slow exchange with water, suggesting an hydrogen bond formation from the NH of Cys6 to the CO of Thr9. The second turn involves residues Thr20 and Gly21 but could not be characterized further due to strong overlap in the NH region for these residues. The third turn involves residues Asn29 and Lys30 and was defined above as a type 1 β-turn. The last turn is found at residues Tyr35 and Gly36. The lack of cross-peaks in this region did not allow the identification of the turn type. However, the low-temperature coefficient obtained for Tyr35 NH together with its slow exchange with water suggest that a hydrogen bond is formed between the NH of this residue and the CO of Lys37 or Thr38.

To characterize further the overall structure of the Pi7 toxin, the deviations from the random-coil position of the

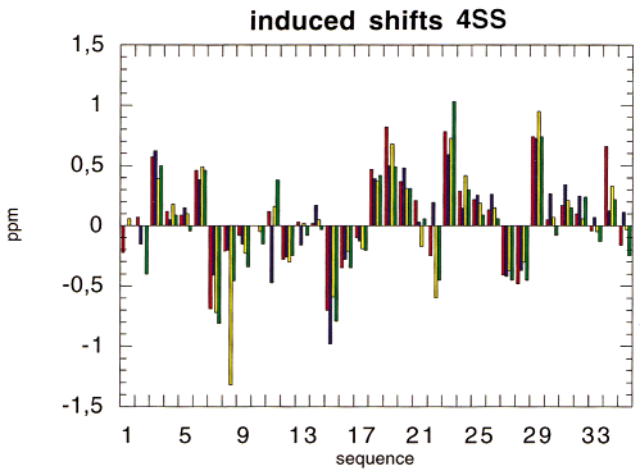

FIGURE 6: Induced shifts of the Hα protons of Pi1 (red), MTX (green), HsTX (blue), and Pi7 (yellow). Induced shifts are deviations of the measured chemical shifts from the random coil values listed in Wishart et al. (*54*).

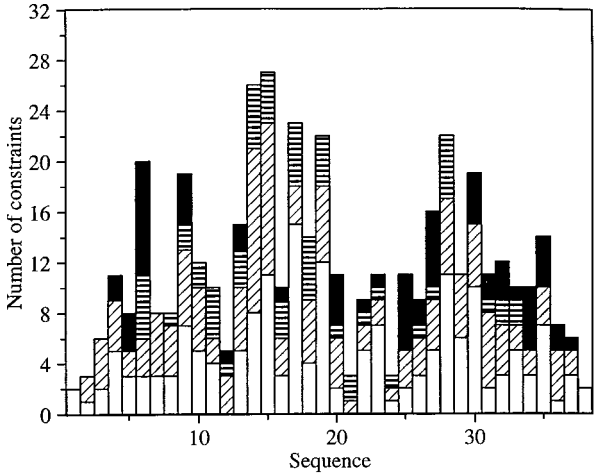

FIGURE 7: Distribution of distance constraints as a function of their residue numbers (white square, intraresidual; diagonally dashed square, sequential; horizontally dashed square, medium range; black square, long range)

Hα chemical shifts were analyzed using the chemical shift index method and compared to other toxins from the same subfamily (*53*). The results for Hα protons are in reasonably good agreement with that expected from other NMR parameters (Figure 6). The α-helical structure can be deduced from residues 8 and 18 while a *β*-sheet is formed by stretches of residues 24−27 and 30−33 and to some extent between residues 4−6. The presence of Pro 15 in the middle of the α helix could explain the deviation observed when using the chemical shift index method for neighboring residues (*54*). The assignment of the Pi7 toxin proton resonances was compared with those of Pi1 (*23*), MTX (*51*), and HsTX1 (*55*). These four toxins, members of the same subfamily, share around 70% primary sequence identity. Although in maurotoxin (MTX) disulfide pairing differs from those of Pi1, Pi7, and HsTX1, the Hα conformational shifts for the four toxins are very similar not to say identical (Figure 6). The largest differences are observed in the environment of aromatic residues, which are not located at the same position.

The backbone amide protons of the Pi7 peptide have highly variable temperature coefficients ranging from 0 to −7.7 ppb per degree (°C). The variations studied in the temperature range from 25 °C to 40 °C are reported in Table S-1. The temperature coefficients are very low, in the order of −4 ppb per degree, from residues Asp11 to Ile19, belonging to the α-helical part of the peptide, whereas an alternance of low and high-temperature coefficients is observed in the *β*-strands. Indeed, the amide protons of the residues 26, 28, 31, and 33 facing each other in the 24−29 and 31−34 *β*-strands have low-temperature coefficients, whereas the coefficients of remaining amide protons are substantially higher. In addition, the amide proton of Cys6 that has been found to exhibit a dipolar interaction with the Ser31 Hα proton also displays a low-temperature coefficient. Comparison of the temperature coefficients with NH exchange rate (Table S-1) shows a good agreement between low coefficient and slow exchange rate with only two exceptions: Ile14 that exchanges slowly with a high-temperature coefficient and Cys22 that exchanges rapidly with a low-temperature coefficient. If we consider that only low coefficients (−4 ppb/°C) (*56*) and slow exchange can be indicative of hydrogen-bond formation, then 10 hydrogen bonds can be proposed (Table S-1), namely, NHs from Cys6, Cys16, Arg17, Tyr18, Ile19, Arg26, Ile28, Ser31, Lys33, and Tyr35.

Finally, a few long-range interactions, such as those observed between Thr9 and Cys27, between Thr18 and Tyr33 and between Tyr35 aromatic protons and Arg26 side chain protons, provide additional constraints for the three-dimensional structure determination.

Structure Calculations. NOESY experiments yielded a set of 310 upper limit constraints, with 174 intra and 136 interresidues of which 73 are sequential, 31 medium range, and 32 long-range giving a total of 210 meaningful upper distance constraints for DYANA. Figure 7 shows the number of experimental NOEs as a function of residue number. The experimental data set contained also 19 ϕ and four $\chi 1$ torsional angle constraints.

Disulfide Bridges. Although, it was proposed to identify disulfide bridges from CHαCH*β* and CH*β*CH*β* connectivities observed between the cysteines involved (*57*, *58*) in cysteine-rich proteins, it is not always possible to reach conclusive results (*59*, *60*). Scorpion venom toxins belong to the cysteine-rich protein family and as expected the CH*β*CH*β* connectivities often involve more than two cysteines. Indeed, if only one interaction is observed between H*β* protons of residues 16 and 34 several are observed from cysteine 6, namely, with cysteines 27 and 32 (Figure 8). This would suggest that cysteines 6, 27, and 32 are in close proximity, whereas the disulfide bridge 16−34 is isolated. The lack of interaction from well resolved cysteine 22 H*β* protons suggests a higher flexibility of the corresponding disulfide bridge. Others H*β* proton interactions could not be analyzed due to overlap. Therefore, a method based on floating assignment of disulfide-bond partners was used to propose topologies compatible with NMR-restraints from the 105 possible combinations of disulfide bridges (*20*).

One hundred and 10 structures with lowest experimental energies (less than 36 kcal/mol) were selected from the total of 220 conformers obtained by the two stages SA protocols with ambiguous restraints on Cys S^{γ} atoms. Thirty structures with nonphysical topologies containing more than four disulfide bridges (*19*, *20*) were excluded of the selected structure ensemble. Two arrangements of the disulfide bridge

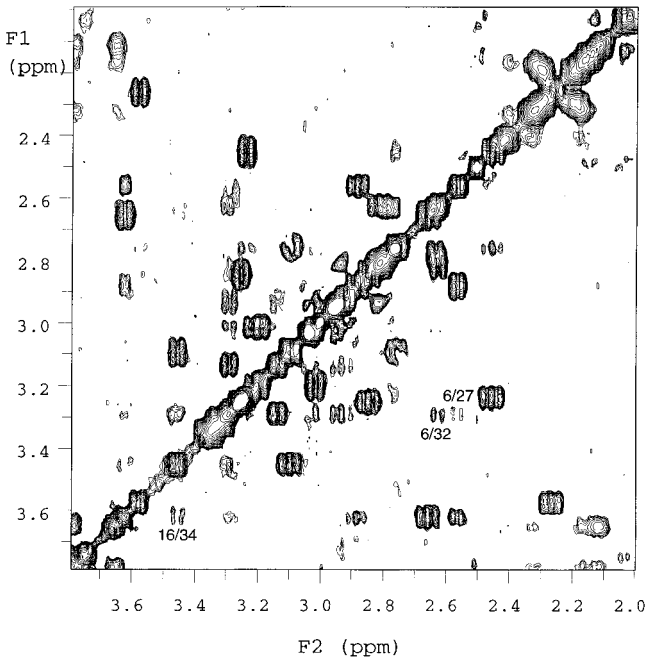

FIGURE 8: Contour plot of the cysteines β proton region of the NOESY spectrum recorded with 250 ms mixing time at 35 °C.

pairings were observed among the remaining 80 structures : (a) 6−27, 12−32, 16−34, and 22−37 in 32 structures; (b) 6−32, 12−27, 16−34, and 22−37 in 48 structures. All eighty calculated structures possess disulfide bridges 16−34 and 22−37. The statistic distribution of distances between sulfur atoms (Figure 9 A) indicates that the topology 6−27, 12−32, 16−22, and 34−37 proposed for the synthetic MTX (*51*) is incompatible with our NMR-restraints. As represented on Figure 9B, the spatial proximity of the four cysteines residues (6, 12, 27, 32) renders virtually impossible the distinction between topology (a) and (b) on the basis of the used NMR-restraints set. We, therefore, used the consensus of the biochemical studies, and considered the topology (a) as the one defining the pairing of disulfide bridges in Pi7.

The experimental NMR constraints together with the additional constraints corresponding to the four disulfide bridges 6−27, 12−32, 16−34, and 22−37 were used as input for the calculation of the preliminary structures as described in structure calculation 1b. Twenty five (from 200) best conformers were analyzed for the formation of hydrogen bonds. From 16 hydrogen bonds appearing in more than two-third of analyzed structures, nine were compatible with both measured temperature coefficients and amide exchange rate. These hydrogen bonds included: Cys6HN-Lys30O, Cys16HN-Cys12O, Tyr18HN-Ile14O, Ile19HN-Pro15O, Arg26HN-Lys33O, Ile28HN-Ser31O, Ser31HN-Ile28O, Lys33HN-Arg26O, and Tyr35HN-Asn24O and were taken as additional constraints for calculation of the final set of conformers. Althougth measured temperature coefficients and amide exchange rate of Arg17 are in favor of an hydrogen bond formation, the Arg17HN-Tyr13O hydrogen bond was not taken into the set as it appeared only in 14 over 25 preliminary structures. A summary of statistics of the final structures obtained with DYANA and OPAL is given in Table 1. The final structures (Figure 10) were consistent with the experimental data having no distance constraints violations greater than 0.1 Å neither torsion angle violations greater than 2.5°. The distribution of ϕ/ψ dihedral angles was 73.8, 22.2, 2.8, and 1.2% of residues in the most favored, allowed, generously allowed and not allowed regions, respectively, of the Ramachandran map. The average value of the circular variance for ϕ/ψ dihedral angles was 0.10 for all residues, and 0.03 for the secondary structure regions.

The regions of secondary structure, defined using the DSSP algorithm, include a helical region spanning from residues 9−20 and an antiparallel β sheet formed by two strands running between the residues 25−28 and 31−34, respectively. An additional β strand appears in the N-terminal part (residues 5−6) of the protein. The helix running from residues 9−20 appears in six final structures and from 13 to 20 in seven final structures. In the remaining structures, the α-helix is well-defined between residues 15−20 as limited by proline residue at position 14 and preceded by another α or 3/10 helix, three to four residues long, or by a series of turns.

In most of the calculated structures, the aromatic ring of Tyr35 lies above the Lys33 side chain as predicted by the upfield shifts observed for some of the Lys33 side chain protons.

Biological Implications. Why Pi7 does not bind or does not affect the function of the K^+-channels thus far studied? A possible answer to this question could reside on its three-dimensional folding, which was the rational taken into consideration for the development of the present work. However, as discussed above, the overall fold of Pi7 peptide is practically identical to that of all other known three-dimensional structures of K^+-channel toxins isolated from scorpion venoms. Thus, the reason for the apparent lack of biological function on K^+-channels should reside on differences at the primary structure level. Another possibility could be that the appropriate target, for which it was selected by natural evolution, is still unknown (*15*). Actually, the two possibilities go together and certainly explain the proper fitness that must exist between a ligand−receptor interaction.

The functional epitope of scorpion toxins specific for K^+-channels have been characterized (*13*, *15*, *61*). One of the important amino acid residues described to be crucial for channel recognition is Lys27 in ChTX (*62*), or Lys28 in NTX (*63*). Similar situations have been described for KTX, AgTX, and others (*61*). The epsilon amino group of the side-chain is taking the place of potassiun ions, inside the pore of the channel at the central position of the channel symmetry axis (*8*). In Pi7, this lysine is replaced by an arginine and represents an unique case of such modification, among all known toxins, with the only exception of BomPO2 (*64*), which has Thr at this position. Although this might be enough to justify the lack of apparent recognition of Pi7 for K^+-channels, it is somehow surprising, since the substitution of Lys27 for Arg27 in ChTX only reduces its affinity by a factor of 1400 (*62*, *65*). The effect of Pi7 has not been tested at higher concentrations, and we cannot rule out that at low micromolar concentrations, Pi7 will not have some activity. It is worth mentioning that recombinant mutants of NTX (*63*), from the subfamily 2 (*14*), in which an Arg28 substitutes for Lys28, shifted the binding constant by a factor of 3 units of logarithm less than the native NTX, when assayed in Kv1.1 channels expressed in oocytes. However, the K28R mutant display the same affinity as the native NTX in synaptosomal membranes. Only when the NTX mutant

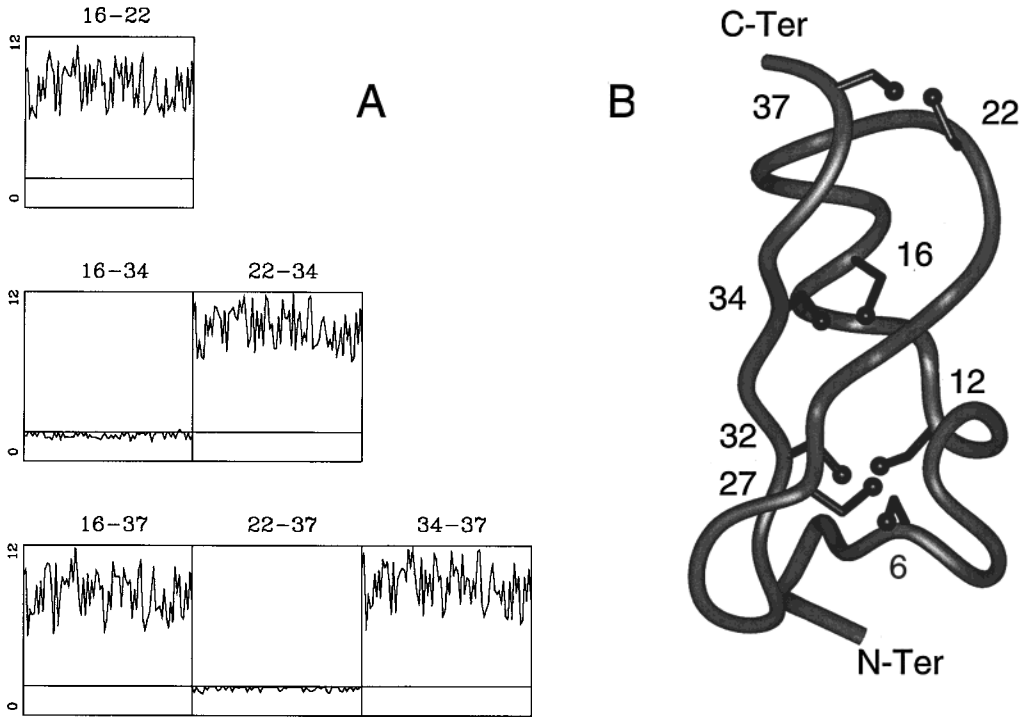

FIGURE 9: NMR Determination of the disulfide bridge topology**.** (A) Distribution of the distances between cysteine 16, 22, 34, and 37 sulfur atoms for the selected structure ensemble. The *x*-axis corresponds to each of the 80 conformers of the ensemble. The *y*-axis corresponds to the distance (from 0 to 12 Å) between S atoms of the cysteines labeled in the graph title. Normal S−S distance for a disulfide bridge (2.03 Å) are shown as horizontal lines. (B) Global fold and distribution of the cysteine side chains in the Pi7 toxin. The backbone of selected structure characterized by the lowest experimental energy is represented by a gray ribbon. Cysteine side chains are represented in black and labeled by their sequence number.

Table 1: Experimental Constraints[a] and Structural Statistics

experimental distance constraints (upper limits):											
intraresidue		sequential		medium range		long range		total			
174		73		31		31		310			
25 best DYANA structures											
violations											
		upper limits		lower limits		vdW		torsion angle		RMSD	
	target function (Å^2)	sum (Å)	max (Å)	sum (Å)	max (Å)	sum (Å)	max (Å)	sum (deg)	max (deg)	bb (Å)	heavy (Å)
ave	0.35	1.8	0.21	0.2	0.0	1.1	0.16	0.1	0.02	1.55	2.35
±	2.98×10^2	0.2	0.03	0.1	0.02	0.2	0.02	0.0	0.01	0.34	0.34
min	1.29	1.5	0.15	0.0	0.01	0.8	0.11	0.0	0.01	0.71	1.65
max	0.39	2.2	0.30	0.3	0.11	1.5	0.20	0.1	0.03	2.64	3.63
25 structures after restrained energy minimization in water (OPAL)											
violations											
	energy (Kcal/mol)	upper limit				torsion angles				RMSD	
		sum (Å)		max (Å)		sum (deg)		max (deg)		bb (Å)	heavy (Å)
ave	−1349.17	1.20		0.09		5.38		1.53		1.68	2.54
±	43.75	0.09		0.01		2.05		0.26		0.33	0.33
min	−1478.08	1.06		0.08		2.68		1.14		0.94	1.78
max	−1264.60	1.40		0.10		10.52		2.01		2.86	3.77

[a] Angle constraints: ϕ: 19; χ1: 4. [b] The set of distance constraints included experimental constraints as well as those corresponding to disulfide bridges and to hydrogen bonds. The energy statistics for the minimized structures concerns the contributions from solute−solute interactions to the potential energy.

had a Glu28 replacing Lys28, was the binding constant decreased by about 1,000-fold compared to the native NTX, in both preparations, (*63*). A similar situation was encountered for the Iberiotoxin (subfamily 1), a high-affinity blocker of the large-conductance, calcium-activated channel (maxi-K or BK), for which the mutation K27R (ChTX numbering) induces only a small increase of the K_d from 1.7 to 6.8 nM (*66*). Thus, the affinity depends not only on the primary structure of the toxin, but also on the type or subtypes of channel being tested.

Apart from the critical Lys27, few other residues were shown to be important for ChTX interaction with the cal-

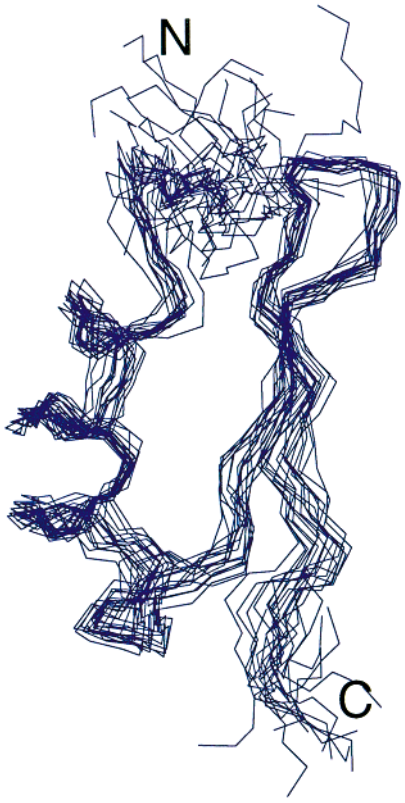

FIGURE 10: Backbone representation of the twenty-five best structure of Pi7 peptide with backbone superposition carried out for residues 4−37 (MOLMOL). The global RMSD calculated over all residues is 1.68 Å for backbone atoms and 2.54 Å for all heavy atoms. The poor overall values are due to the small number of meaningful constraints per residues available (6.3 per residue, including disulfide bridges and hydrogen bonds). Both N- and C-terminal suffer particularly from the lack of constraints in these regions, and the backbone RMSD decreases to 1.06 ± 0.20 Å when only the residues 4−37 are taken into account. The RMSD values calculated over the secondary structure elements (residues 5−6, 9−20, 25−28, 31−34) are 0.84 and 1.69 Å for backbone and heavy atoms, respectively.

cium-activated potassium channel, namely, Ser10, Trp14, Arg25, Lys27, Met29, Asn30, Arg34, and Tyr36 (*67*). Five residues are critical for the recognition of the shaker K^+-channel: Lys27, Met29, Asn30, Arg34, and Tyr36, (*65*). However, the role of other residues in the affinity of K^+-toxins for voltage-dependent potassium channels should not be neglected. Indeed, the two toxins Pi2 and Pi3 from subfamily 7 differ only in position 7 (position 10 of ChTX numbering), where a proline in Pi2 is changed by a glutamic acid in Pi3. This change causes a seventeen folds decrease affinity for Pi3 (*68*).

Other amino acid residues situated at the N- and C-terminal regions of K^+-channel specific toxins were shown to be important for channel recognition (*69*−*73*). These include amidation of the last C-terminal amino acid (*14*, *70*) or blocked N-terminal residues (pyroglutamic acid) as it is the case for toxin of subfamily 1 (*15*). Most K^+-channel specific toxins have hydrophobic amino-terminals as in subfamily 2 (*15*). Pi7 is unique in having two highly negatively charged amino acids at the extreme N-terminal. Also, in the case of the sea anemona toxin BgK, a K^+-channel blocking toxin with a different three-dimensional folding, a tyrosine in position 36 was assumed to be as important as the Lys27 for its function (*69*). In the case of Pi7, this Tyr is, however, present, which makes the corresponding tyrosine of Pi7 not that important when compared to BgK (*69*).

Finally, one of the most significant difference might reside on the net positive charge value of the peptide. For the case of Pi7, a charge of +3 was calculated, which makes it the least basic peptide of all the peptides in subfamily 6. Unless, there is still an unknown subtype of K^+-channels for which Pi7 was evolved and maintained in *Pandinus imperator* venom, it could well be that afterall, the electrostatic interactions of the entire molecule with the channels are responsible for its low affinity to the ion-channels tested thus far.

ACKNOWLEDGMENT

We thank M.Sc. Timoteo Olamendi-Portugal for the purification of Pi7 toxin. J. B. thanks Drs D. Marion and M. Blackledge for invaluable advice.

SUPPORTING INFORMATION AVAILABLE

A table of proton chemical shifts with $^3J_{NH-H\alpha}$ coupling constants and amide proton exchange rates. This material is available free of charge via the Internet at http://pubs.acs.org.

REFERENCES

1. Catterall, W. A. (1980) *Annu. Rev. Pharmacol. Toxicol. 20*, 15−43.
2. Dehesa-Davila, M., and Possani, L. D.(1994) *Toxicon 32*, 1015−1018.
3. Gordon, D., Savarin, P., Gurevitz, M., and Zinn-Justin, S. (1998) *J. Toxicol-Toxin Reviews 17*, 131−159.
4. MacKinnon, R., Heginbothan, L., and Abramson, T. (1990) *Neuron 5*, 767−771.
5. MacKinnon, R., Aldrich, R. W., and Lee, A. W. (1993) *Science 262*, 757−759.
6. Olivera, B. M., Hillyard, D. R., Marsh, M., and Yoshikami, D. (1995) *Trends Biotechnol. 13*, 422−426.
7. MacKinnon, R. (1991) *Nature 350*, 232−235.
8. Doyle, D. A., Cabral, J. M., Pfuetzner, R. A., Kuo, A., Gulbis, J. M., Cohen, S. L., Chait, B. T., and MacKinnon, R. (1998) *Science 280*, 69−77.
9. Gurrola, G. B., Rosati, B., Rocchetti, M., Pimienta, G., Zaza, A., Arcangeli, A., Olivotto, M., Possani, L. D., and Wanke, E. (1999) *FASEB J. 13*, 953−962.
10. Possani, L. D., Martin, B. M., and Svendsen, I. (1982) *Carlsberg Res. Commun. 47*, 285−289.
11. Dauplais, M., Gilquin, B., Possani, L. D., Gurrola-Briones, G., Roumestand, C., and Menez, A. (1995) *Biochemistry 34*, 16563−16573.
12. Garcia, M. L., Garcia-Calvo, M., Hidalgo, P., Lee, A., and Mackinnon, R. (1994) *Biochemistry 33*, 6834−6839.
13. Miller, C. (1995) *Neuron 15*, 5−10.
14. Selisko, B., Garcia, C., Becerril, B., Gomez-Lagunas, F., Garay, C., and Possani, L. D. (1998) *Eur. J. Biochem 254*, 468−479.
15. Possani, L. D., Selisko, B., Gurrola, G. B. (1999) *Perspectives Drug Discovery Design 15/16*, 15−40.
16. Sissom, W. D. (1990) *The Biology of Scorpions* (Gary A. Polis, Ed.) Stanford University Press, Stanford, California. Systematics, Biogeography, Paleontology.
17. Olamendi-Portugal, T., Gomez-Lagunas, F., Gurrola, G. B., and Possani, L. D. (1998) *Toxicon 36*, 759−770.
18. Peter, M., Jr., Varga, Z. J., Panyi, G., Bene, L., Damjanovich, S., Pieri, C., Possani, L. D., and Gaspar R. J. (1998) *Biochem. Biophys. Res. Comm. 242*, 621−625.
19. Nilges, M. (1995) *J. Mol. Biol. 245*, 645−660.
20. Boisbouvier, J., Albrand, J.-P., Blackledge, M., Jaquinod, M., Schweitz, H., Lazdunski, M., and Marion, D. (1998) *J. Mol. Biol. 283*, 205−219.

21. Dent, M. A. R., Possani, L. D., Ramirez, G. A., and Fletcher, P. L., Jr. (1980) *Toxicon 18*, 343−350.
22. Manzi, A., Salimath, P. V., Spiro, R. C., Keifer, P. A., and Freeze, H. H. (1995) *J. Biol. Chem. 270*, 9154−9163.
23. Delepierre, M., Prochnicka-Chalufour, A., and Possani, L. D. (1997) *Biochemistry 36*, 2649−2658.
24. Delepierre, M., Prochnicka-Chalufour, A., and Possani, L. D. (1998) *Toxicon 36*, 1599−1608.
25. States, D. J., Haberkorn, R. A., and Rubens, D. J. (1982) *J. Magn. Reson. 48*, 286−292.
26. Braunschweiler, L., and Ernst R. R. (1983) *J. Magn. Reson. 53*, 521−528.
27. Bax, A., and Davis, D. G. (1985) *J. Magn. Reson. 65*, 355−360.
28. Griesinger, C., Wüthrich, K., and Ernst, R. R. (1988) *J. Am. Chem. Soc. 110*, 7870−7892.
29. Boyd, J., Dobson, C. M., and Redfield, C., (1983) *J. Magn. Reson. 55*, 170−176.
30. Kumar, A., Ernst, R. R., and Wüthrich, K. (1980) *Biochem. Biophys. Res. Commun. 95*, 1−6.
31. Kupce, E., and Freeman, R. (1995) *J. Magn. Reson., Series A 115*, 273−276.
32. Kupce, E., Schmidt, P., Rance, M., and Wagner, G. (1998) *J. Magn. Reson. 135*, 361−367.
33. Güntert, P., Mumenthaler, C., and Wüthrich, K. (1997). *J. Mol. Biol. 273*, 283−298.
34. Luginbühl, P., Güntert, P., Billeter, M., and Wüthrich, K. (1996). *J. Biomol. NMR, 8*, 136−146.
35. Bartels, C., Xia, T., Güntert, P., Billeter, M., and Wüthrich, K. (1995). *J. Biomol. NMR 5*, 1−10.
36. Szyperski, T., Güntert, P., Otting, G., and Wüthrich, K. (1990) *J. Magn. Reson. 99*, 552−560.
37. Mumenthaler, C., and Braun, W. (1995) *J. Mol. Biol. 254*, 466−480.
38. Blackledge, M. J., Medvedeva, S., Poncin, M., Guerlesquin, F., Bruschi, M., and Marion, D. (1995). *J. Mol. Biol*., *245*, 661−681.
39. Boisbouvier, J., Blackledge, M., Sollier, A., and Marion, D. (1999), submitted.
40. Cornell, W. D., Ciepak, P., Bayly, C. I., Gould, I. R., Merz, K. M., Jr., Ferguson, D. M., Spellmayer, D. C., Fox, T., Caldwell, J. W., and Kollman, P. A. (1995) *J. Am. Chem. Soc. 117*, 5179−5197.
41. Koradi, R., Billeter, M., and Wüthrich, K. (1996) *J. Mol. Graphics 14*, 51−55.
42. Laskowski, R. A., MacArthur M. W., Moss, D. S., Thornton, J. M. (1993). *J. Appl. Crystallogr. 26*, 283−291.
43. Wüthrich, K. (1986) *NMR of Proteins and Nucleic Acids*, Jonh Wiley and sons, New York.
44. Delepierre, M, Kupce, E. and Kiefer, P (2000), to be published.
45. Bontems, F., Roumestand, C., Gilquin, B., Menez, A., and Toma F., (1991a) *Science 254*, 1521−1523.
46. Song, J., Gilquin, B., Jamin, N., Drakopoulou, E., Guenneugues, M., Dauplais, M., Vita, C. and Ménez, A. (1997) *Biochemistry, 36*, 3760−3766.
47. Johnson, B. A., Stevens, S. C., and Williamson, J. M. (1994) *Biochemistry 33*, 15061−15070.
48. Fernandez, I., Romi, R., Szendeffy, S., Martin-Eauclaire, M.-F., Rochat, F., Van Rietschoten, J., Pons, M., and Giralt, E. (1994) *Biochemistry 33*, 14256−14263.
49. Krezel, A. M., Kasibhatla, C., Hidalgo, P., MacKinnon, R., and Wagner, G. (1995) *Protein Sci. 4*, 1478−1489.
50. Blanc, E., Fremont, V., Sizun, P., Meunier, S., Van Rietschoten, J., Thevand, A., Bernassau, J.-M., and Darbon, H. (1996) *Proteins: Struct., Funct. Gen. 24*, 359−369.
51. Blanc, E., Sabatier, J. M., Kharrat, R., Meunier, S., El Ayeb, M., Van Rietschoten, J., and Darbon, H. (1997) *Proteins: Struct., Funct. Gen. 29*, 321−333.
52. Johnson, B. A., and Sugg, E. E. (1992) *Biochemistry 31*, 8151−8159.
53. Wishart, D. S., Sykes, B. D., and Richards, F. M. (1992) *Biochemistry 31*, 1647−1651.
54. Wishart, D., Bigam, C. G., Holm A., Hodges, R. S., and Sykes, B. D. (1995) *J. Biomol. NMR 5*, 67−81.
55. Savarin, P., Romi-Lebrun, R., Zinn-Justin, S., Lebrun, B., Nakajima, T., Gilquin, B., and Ménez, A. (1999) *Protein Sci.*, in press.
56. Temussi, P. A., Tancredi, T., Pastore, A., and Castiglione-Morelli, M. A. (1987) *Biochemistry 26*, 7856−7863.
57. Williamson, P. M., Havel, T. F., and Wüthrich, K. (1985) *J. Mol. Biol. 182*, 295−315.
58. Adler, M., Lazarus, R. A., Dennis, M. S., and Wagner, G. (1991) *Science 253*, 445−448.
59. Heitz, A., Chiche, L., Le-Nguyen, D., and Castro, B. (1989) *Biochemistry 28*, 2392−2398.
60. Klaus, W., Broger, C., Gerber, P., and Senn, H. (1993) *J. Mol. Biol. 232*, 897−906.
61. Garcia, M. L., Hanner, M., Knaus, H. G., Koch, R., Schmalhofer, W., Slaughter, R. S., and Kaczorowski, G. J. (1997) *Adv. Pharmacol. 39*, 425−471.
62. Park, C. S., and Miller, C. (1992) *Neuron 9*, 307−313.
63. Martinez, F., Munoz-Garay, C., Gurrola, G., Darszon, A., Possani, L. D., and Becerril, B. (1998) *FEBS Lett. 429*, 381−384.
64. Romi-Lebrun, R., Martin-Eauclaire, M. F., Escoubas, P., Wu, F. Q., Lebrun, B., Hisada, M., and Nakajima, T (1997) *Eur. J. Biochem 245*, 447−464.
65. Golstein, S. A. N., Pheasant, D. J., and Miller, C. (1994) *Neuron 12*, 1377−1388.
66. Mullmann, T. J., Munujos, P., Garcia, M. L., and Giangiacomo, K. M. (1999) *Biochemistry, 38*, 2395−2402.
67. Stampe, P., Kolmakova-Partensky, L., and Miller, C. (1994) *Biochemistry 33*, 443−450.
68. Gomez-Lagunas, F., Olamendi-Portugal, T., Zamudio, F. Z., and Possani, L. D. (1996) *J. Membrane Biol. 152*, 49−56.
69. Dauplais, M., Lecoq, A., Song, J., Cotton, J., Jamin, N., Gilquin, B., Roumestand, C., Vita, C., de Medeiros, C. L. C., Rowan, E., G., Harvey, A. L., and Ménez, A. (1997) *J. Biol. Chem. 272*, 4302−4309.
70. Lebrun, R., Romi-Lebrun, R., Marin-Eauclaire, M.-F, Yasuda, A., Ishiguro, M., Oyama, Y., Pongs, O., and Nakajima, T. (1997) *Biochem. J. 328*, 321−327.
71. Gurrola, G. B., Molinar-Rode, R., Sitges, M., Bayon, A., and Possani, L. D. (1989) *J. Neural Transmission 77*, 11−20.
72. Vaca, L., Gurrola, G. B., Possani, L. D., and Kunze, D. L. (1993) *J. Membrane Bio. 134*, 123−129.
73. Gurrola, G. B., and Possani, L. D. (1995) *Biochem. Mol. Biol. Intern. 37*, 527−535.

BI991685M